Growth of $Si_{1-x}Ge_x(011)$ on Si(011)16×2 by gas-source molecular beam epitaxy: Growth kinetics, Ge incorporation, and surface phase transitions

N. Taylor, H. Kim, T. Spila, J. A. Eades,[a] G. Glass,
P. Desjardins, and J. E. Greene[b]
Materials Science Department, Coordinated Science Laboratory, and Materials Research Laboratory, University of Illinois, 1101 West Springfield Avenue, Urbana, Illinois 61801

(Received 8 June 1998; accepted for publication 1 October 1998)

Single crystal $Si_{1-x}Ge_x(011)$ layers with $x \leqslant 0.35$ have been grown on double-domain Si(011)''16×2'' surfaces from Si_2H_6/Ge_2H_6 mixtures at temperatures $T_s = 400-950\,^\circ$C. D_2 temperature programmed desorption was used to show that the structure of the Si(011)''16×2'' surface unit cell, more correctly written as $\begin{bmatrix} 17 & 1 \\ 2 & 2 \end{bmatrix}$ since the unit cell vectors are nonorthogonal, is composed of 16 adatoms and eight π-bonded dimers with a dangling bond density half that of the 1×1 surface. $Si_{1-x}Ge_x(011)$ overlayers are ''16×2'' when $x < x_c(T_s)$ and ''2×8'' with $x > x_c(T_s)$. The value of x_c decreases from $\simeq 0.10$ at $T_s = 475\,^\circ$C to 0.08 at 550 °C to 0.06 at 650 °C. Both the ''2×8'' and ''16×2'' $Si_{1-x}Ge_x(011)$ surface reconstructions gradually and reversibly transform to 1×1 at T_s between 650 and 725 °C. Film growth kinetics exhibit three distinct regimes. At low temperatures ($T_s \lesssim 500\,^\circ$C), the film deposition rate R_{SiGe} decreases exponentially with $1/T_s$ in a surface-reaction-limited growth mode for which the rate-limiting step is hydrogen desorption from Si and Ge monohydride phases. R_{SiGe} becomes essentially constant with T_s in the intermediate impingement-flux-limited range, $T_s = 500-650\,^\circ$C. At $T_s > 650\,^\circ$C, R_{SiGe} increases again with T_s due initially ($T_s \simeq 650-725\,^\circ$C) to an increase in the steady-state dangling bond coverage as the surface reconstruction gradually transforms to 1×1. The continued increase in R_{SiGe} at even higher T_s is associated with strain-induced roughening. Ge/Si ratios in as-deposited films are linearly proportional to the incident Ge_2H_6/Si_2H_6 flux ratio $J_{Ge_2H_6}/J_{Si_2H_6}$ and nearly independent of T_s indicating that the reactive sticking probabilities of Si_2H_6 and Ge_2H_6 have very similar temperature dependencies. $R_{SiGe}(J_{Ge_2H_6}/J_{Si_2H_6}, T_s)$ in both the surface-reaction-limited and flux-limited regimes is well described by a simple kinetic model incorporating second-order dissociative chemisorption and second-order hydrogen desorption as rate-limiting steps.

I. INTRODUCTION

Gas-source molecular beam epitaxy (GS-MBE) has been shown to provide several advantages over solid-source MBE for the growth of Si and $Si_{1-x}Ge_x$ alloys. These include: elimination of hot crucibles and the change in deposition rate associated with charge depletion, higher sample throughput, better conformal coverage, better lateral film thickness uniformity, and the potential for selective epitaxy on patterned substrates. While initial GS-MBE experiments were carried out using SiH_4 and GeH_4, more recent results have demonstrated that the use of Si_2H_6 and Ge_2H_6 as precursors for Si[1] and Ge[2] growth yields reactive sticking probabilities up to two orders of magnitude higher. This is primarily due to the ease of cleaving IV–IV, compared to IV–H, bonds. Predictive models of the growth rates of GS-MBE Si,[1] Ge,[2] and $Si_{1-x}Ge_x$[3] on Si(001) as functions of incident fluxes and deposition temperatures have been developed based upon dissociative chemisorption of the dihydride molecules followed by a series of surface decomposition reactions with the final step being hydrogen desorption from Si and/or Ge monohydride. The models exhibit very good agreement with experimental results. In the case of $Si_{1-x}Ge_x(001)$ growth, Ge segregation as a function of steady-state hydrogen coverage is also accounted for.[3,4]

$Si_{1-x}Ge_x$/Si(011) offers potential benefits over $Si_{1-x}Ge_x$/Si(001) for certain types of device applications. Strained $Si_{1-x}Ge_x$/Si(011) heterostructures have additional degrees of freedom for band gap engineering: the maximum film/substrate conduction-band offset is predicted to be substantially larger,[5] the optical band gap decreases more rapidly with increasing x,[5] and optical selection rules allow hole–intersubband transitions to be excited by light polarized parallel to $Si_{1-x}Ge_x$/Si(011) multiple quantum well layers.[6] The $Si_{1-x}Ge_x$/Si(011) system also exhibits novel dislocation structures and highly asymmetric in-plane strain relaxation. While $a/2\langle 110\rangle$ misfit dislocation glide is allowed on all $\{111\}$ planes along all $\langle 110\rangle$ interfacial directions in $Si_{1-x}Ge_x$/Si(001) heterostructures, they are constrained to glide only on $(\overline{1}11)$ and $(11\overline{1})$ planes and only along one $\langle 110\rangle$ in-plane direction, $[1\overline{1}0]$, in $Si_{1-x}Ge_x$/Si(011).[7]

Another striking difference between $Si_{1-x}Ge_x(011)$ and $Si_{1-x}Ge_x(001)$, which has a significant effect on film growth

[a]Present address: Department of Materials Science and Engineering, Lehigh University, 5 East Packer Avenue, Bethlehem, PA 18015.
[b]Electronic mail: jegreene@uiuc.edu

kinetics and mechanistic rate limitations during gas-source film growth, is the higher complexity of the $Si_{1-x}Ge_x(011)$ surface unit cell. Initial reflection high-energy electron diffraction (RHEED) and low-energy electron diffraction (LEED) studies of the Si(011) surface revealed a variety of reconstructions, including 2×1, 4×5, 5×1, 7×1, 9×1, ''*X*,'' and faceted structures.[8,9] However, subsequent LEED and Auger electron spectroscopy (AES) results by Ichinokawa *et al.*[10] demonstrated that all are due to Ni contamination and that the clean Si(011) surface has a complex reconstruction which they termed ''16×2.'' Yamamoto *et al.*[11] confirmed the Ni-induced reconstructions and reported a ''16-structure'' for the clean surface.

Based upon an analysis of LEED results, Ampo *et al.*[12] proposed that the Si(011) clean-surface reconstruction is ''16×2'' with a unit cell composed of upper and lower terraces of equal widths and separated by single-atom-height steps along the $[2\bar{1}1]$ direction. Miura *et al.*[13] demonstrated that the Si(011) surface structure, while labeled ''16×2'' based upon observed diffraction pattern periodicities, actually has a $\left[\begin{smallmatrix}17 & 1\\ 2 & 2\end{smallmatrix}\right]$ reconstruction. This was verified by van Loenen *et al.*[14] using scanning tunneling microscopy (STM). The detailed atomic configurations on the upper and lower terraces were, however, still unknown. Proposed configurations include structures in which the surface atoms form dimers and trimers,[15] adatoms,[16,17] or adatoms and dimers.[18–20] Recently, Kim *et al.*[21] used temperature programmed desorption (TPD) to show that the Si(011) surface unit cell is composed of adatoms and dimers.

Ichinokawa *et al.*[10] found, based upon LEED results, that the ''16×2'' surface reconstruction undergoes a gradual and reversible transition to 1×1 during high temperature annealing. The transition temperature, as determined by LEED and RHEED investigations, was reported as 760 °C by both Yamamoto *et al.*[11] and Shimaoka.[22] In a later article, Yamamoto *et al.*[23] observed, using STM, that the ''16×2'' to 1×1 transformation starts at 710 °C and is complete at 770 °C.

Much less data are available on the surface structure of $Si_{1-x}Ge_x(011)$, and local atomic configurations are completely unknown. Miura *et al.*[13] used LEED and AES to show that depositing Ge, with coverages θ_{Ge} up to 4.1 ML, on Si(011) and post-annealing for one minute at 650 °C results in Ge/Si intermixing which in turn gives rise to several reversible temperature-dependent surface phase transitions upon subsequent heating. The ''16×2'' reconstruction was obtained with $\theta_{Ge}<0.3$ ML and $T<720$ °C, a $\left[\begin{smallmatrix}10 & -1\\ 3 & 4\end{smallmatrix}\right]$ reconstruction at $0.3<\theta_{Ge}<0.7$ ML with $T<640$ °C, and a $\left[\begin{smallmatrix}8 & 0\\ 2 & 1\end{smallmatrix}\right]$ reconstruction at 0.8 ML$<\theta_{Ge}<4.1$ ML with $T<620$ °C. At higher temperatures, all three reconstructions transformed to 1×1. Butz and Lüth[24] used STM to investigate the surface structure of $Si_{1-x}Ge_x$ films grown by solid-source MBE. $Si_{1-x}Ge_x$ layers with $x\leqslant0.06$ had surface terraces of width 3.9 nm, with step edges along $[1\bar{1}\bar{3}]$ and $[1\bar{1}3]$, while the terraces of films with $x\geqslant0.10$ were only 1.9 nm wide with step edges along $[\bar{1}12]$.

There are no detailed studies in the literature on the growth kinetics of Si or $Si_{1-x}Ge_x$ deposited on Si(011) by gas-source techniques. Liu *et al.*[5] reported the deposition of $Si_{1-x}Ge_x(011)$ films by rapid-thermal chemical vapor deposition from $SiCl_2H_2$ and GeH_4 at $T_s=625$ °C and found that, compared to deposition on Si(001) substrates, the 011 film growth rate R_{SiGe} was a factor of two to three times lower although the Ge content x was similar. Both R_{SiGe} and x increased with increasing GeH_4 flow rates.

In this article, we present the results of an investigation of composition- and temperature-dependent surface phase transitions and their role in controlling the kinetics of $Si_{1-x}Ge_x(011)$ growth by GS-MBE from Si_2H_6 and Ge_2H_6. All films were deposited on Si(011) at $T_s=400-950$ °C with dihydride precursor fluxes $J_{Si_2H_6}=2.2\times10^{16}$ cm^{-2} s^{-1} and $J_{Ge_2H_6}=0-7.8\times10^{14}$ cm^{-2} s^{-1}. D_2 TPD analyses reveal that the unit cell of the Si(011)''16×2'' reconstructed surface consists of 16 adatoms and eight π-bonded dimers with a maximum dangling bond density which is only half that of the 1×1 structure. RHEED and LEED results show that the Si(011)''16×2'' surface gradually transforms to a bulk terminated 1×1 structure over a temperature range between 700 and 725 °C. $Si_{1-x}Ge_x(011)$ films grown on Si(011) at temperatures below the 1×1 transition have the ''16×2'' surface reconstruction at low Ge concentrations but transform to a ''2×8'' reconstruction at a critical concentration x_c which ranges from $\simeq0.10$ at $T_s=475$ °C to 0.06 at $T_s=650$ °C. Both the ''16×2'' and ''2×8'' $Si_{1-x}Ge_x(011)$ surface reconstructions also transform reversibly to 1×1. The transformation temperature range varies from $\simeq700-725$ °C at low Ge concentrations to 650–725 °C for $Si_{0.65}Ge_{0.35}$.

For a given $J_{Ge_2H_6}/J_{Si_2H_6}$ flux ratio, $Si_{1-x}Ge_x(011)$ growth kinetics are characterized by three primary temperature regimes. At low temperatures, growth proceeds in a surface-reaction-limited mode in which the rate-limiting step is hydrogen desorption from the monohydride phase and $\log(R_{SiGe})\propto1/T_s$. In the intermediate temperature range, film growth is limited by the flux impingement rate and is essentially independent of T_s. At higher temperatures, R_{SiGe} increases again as the $Si_{1-x}Ge_x$ surface reconstruction gradually transforms to 1×1 with a higher surface dangling bond density. $R_{SiGe}(J_{Ge_2H_6}/J_{Si_2H_6},T_s)$ results in the surface-reaction and flux-limited regimes are well described by a simple kinetic model incorporating second-order dissociative chemisorption and hydrogen desorption as rate-limiting steps.

II. EXPERIMENTAL PROCEDURE

All films were grown in a multichamber ultra-high-vacuum system (described in detail in Refs. 2 and 25) evacuated using a combination of ion and turbomolecular pumps to provide a base pressure of 5×10^{-11} Torr. The GS-MBE system contains a film growth chamber equipped with an *in situ* RHEED apparatus. A sample transfer chamber connects to an analytical chamber with provisions for TPD, LEED, AES, and electron energy loss spectroscopy (EELS).

The film growth experiments were carried out at temperatures $T_s=400-950$°C using a Si_2H_6 flux $J_{Si_2H_6}=2.2\times10^{16}$ cm^{-2} s^{-1} and Ge_2H_6 fluxes $J_{Ge_2H_6}=0-7.8\times10^{14}$ cm^{-2} s^{-1}. During deposition, the Si_2H_6 and Ge_2H_6 molecular

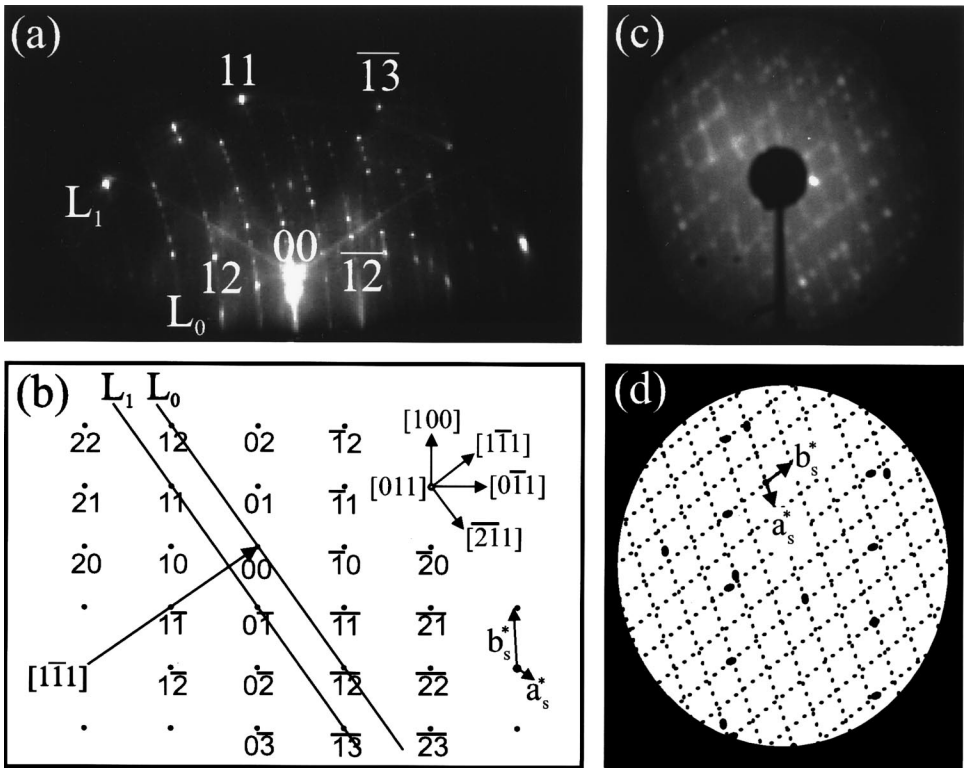

FIG. 1. (a) RHEED pattern obtained along the $[1\overline{1}1]$ azimuth of a 300 °C Si(011)''16×2'' surface. (b) Schematic Si(011) reciprocal space map showing segments of the L_0 and L_1 Ewald spheres. $\overline{a_s^*}$ and $\overline{b_s^*}$ are unit vectors along the edges of the ''16×2'' reciprocal-space surface unit cell. (c) LEED pattern, obtained with a 42.8 eV primary electron beam, from a 300 °C Si(011)''16×2'' surface. (d) Simulated LEED pattern.

beams are delivered to the substrate through individual, directed tubular dosers located 3 cm from the substrate at an angle of 45°. The dosers are coupled to feedback-controlled constant-pressure reservoirs in which pressures are separately monitored using capacitance manometers. Valve sequencing, gas flows, and substrate temperature are all computer controlled.

The substrates used in these experiments were 1×3 cm^2 plates cleaved from 0.38-mm-thick *n*-type (resistivity=0.5–2.0 Ω cm) Si(011) wafers with a miscut of 0.36° along $[\overline{7}72]$. Initial cleaning consisted of degreasing by successive rinses in trichloroethane, acetone, propanol, and deionized (DI) water followed by four consecutive oxidation/etch cycles composed of a 2 min dip in an oxidizing solution of 6:1:1 H_2O:HCl:H_2O_2, a 30 s rinse in DI water, a 20 s etch in dilute (2%) HF, and a final 30 s rinse in fresh DI water. The substrates were then blown dry in ultra-high-purity N_2, exposed to a UV ozone treatment in which they were irradiated from a low-pressure Hg lamp (15 mW cm^2) for 30 min in air to remove C-containing species,[26] and introduced into the deposition system. The substrates were heated by direct current to 600 °C and degassed for 5 h, then rapidly heated at 100 °C s^{-1} to 1100 °C for 1 min to remove the oxide. Temperatures were calibrated using chrome-alumel thermocouples and an optical pyrometer. RHEED patterns from substrates subjected to this procedure were sharp ''16×2'', as described in the following section. No residual C or O was detected by AES.

TPD experiments were carried out in the analytical chamber which is equipped with a differentially pumped quadrupole mass spectrometer. As-deposited samples were heated to 200 °C and exposed to atomic deuterium until saturation coverage. (Additional experiments involving H_2 TPD as well as flash heating followed by D_2 TPD were carried out to show that all H was removed by this procedure, even for the lowest growth temperatures used. *In situ* AES results also established that the Ge coverage remained constant during the deuterium site exchange process.). Deuterium, rather than hydrogen, was used in order to reduce the background signal and obtain greater sensitivity. D_2 was delivered through a doser identical to that described above with a hot W filament near the outlet to crack the gas. The samples were placed 2 mm from the 5-mm-diameter hole in the skimmer cone of the mass spectrometer and heated by direct current at a linear rate $\xi=5$ °C s^{-1}.

$Si_{1-x}Ge_x$ film thicknesses and alloy compositions were determined by Rutherford backscattering spectrometry (RBS). The RBS probe beam consisted of 2 MeV He^+ ions incident at 15° to the sample normal with the detector set at a 150° scattering angle. Backscattering spectra were analyzed using the RUMP[27] simulation program. The reported film compositions are accurate to within 2 at. %.

Cross-sectional transmission electron microscopy (XTEM) examinations were carried out using a Philips CM12 microscope operated at 120 kV. Specimens were prepared by gluing two samples film-to-film and then cutting a

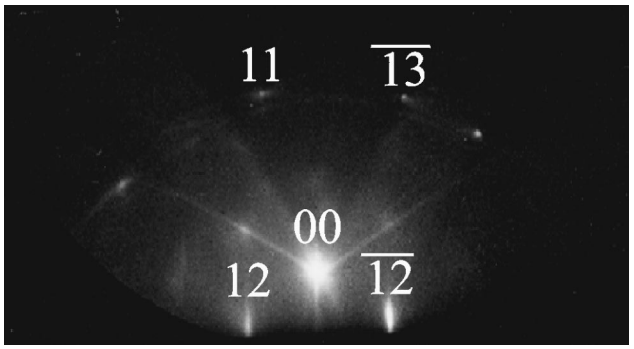

FIG. 2. RHEED pattern obtained along the $[1\overline{1}1]$ azimuth of a 750 °C Si(011) 1×1 surface.

vertical section which was thinned by mechanical grinding to a thickness of $\simeq 25$ μm. Final thinning to electron transparency was done by Ar^+ ion milling. The incident beam angle and energy were progressively reduced from 15° to 11° and from 5 to 3.5 keV, respectively, in order to minimize radiation damage artifacts and to obtain samples with uniform thickness distributions.

III. EXPERIMENTAL RESULTS

A. Si(011)''16×2'' and 1×1 surface reconstructions

The RHEED pattern shown in Fig. 1(a) was obtained along the $[1\overline{1}1]$ azimuth of a clean Si(011) surface. It is composed of well-defined diffraction spots, rather than streaks, with sharp Kikuchi lines and essentially equi-intense fundamental and partial-order reflections indicating an atomically smooth surface with relatively large terraces. The pattern consists of curved rows with 15 partial-order reflections between the fundamental reflections in the zero-order Laue zone L_0 and the corresponding reflections in the first-order Laue zone L_1. (See, for example, the set of partial-order reflections between the specular Bragg reflection labeled 00 in L_0 and the 11 in L_1). The rows along the growth direction are curved because the incident beam is in the $[1\overline{1}1]$ direction while the sides of the reciprocal space unit cell are oriented along [100] and $[\overline{1}1\overline{1}]$. Within each Laue zone arc, there are half-order reflections between every set of fundamental Bragg spots.

Based upon the overall symmetry, this surface reconstruction was originally designated ''16×2''[10] even though in the Wood's surface notation[28] scheme, 16×2 implies that the vectors defining the surface unit cell are orthogonal, which is clearly not the case here. The symmetry is more clearly seen in the reciprocal space map in Fig. 1(b) in which arcs of the L_0 and L_1 Ewald spheres are labeled together with the incident electron beam direction. The reconstruction is $\left[\begin{smallmatrix}17 & 1\\ 2 & 2\end{smallmatrix}\right]$ with real-space unit cell vectors $\overline{a}_s = 17\overline{a} + \overline{b}$ and $\overline{b}_s = 2\overline{a} + 2\overline{b}$. $\overline{a}_s^*$ and $\overline{b}_s^*$ in Figs. 1(b) and 1(d) are the unit vectors along the edges of the reciprocal-space unit cell defined by $\overline{a}_s^* = (\overline{a}^* - \overline{b}^*)/16$ and $\overline{b}_s^* = (-\overline{a}^* + 17\overline{b}^*)/32$. Figures 1(c) and 1(d) are the corresponding experimentally observed (using an electron energy of 42.8 eV) and simulated Si(011)''16×2'' LEED patterns. These results confirm the

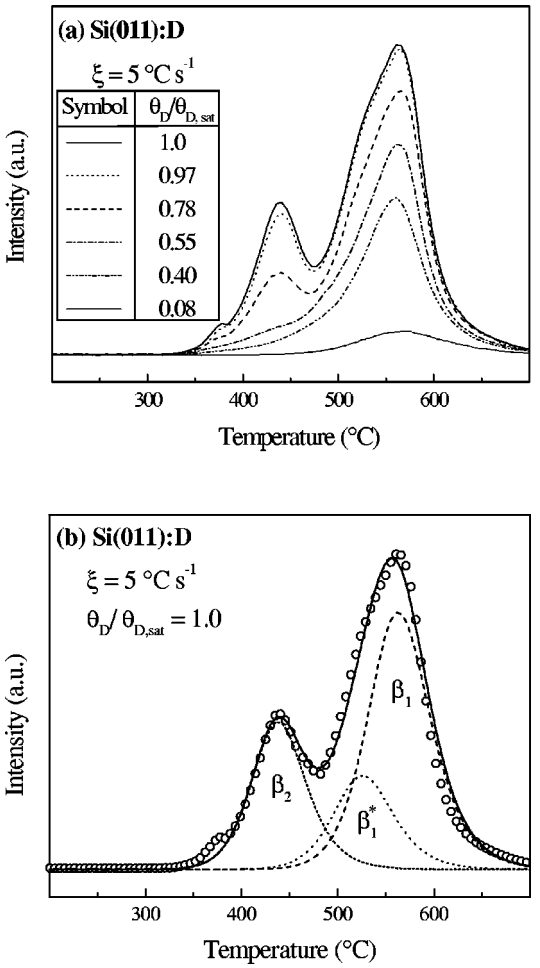

FIG. 3. (a) D_2 TPD spectra from Si(011) surfaces with relative deuterium coverages $\theta_D/\theta_{D,sat} = 1.0$, 0.97. 0.78, 0.55, 0.40, and 0.08. $\theta_{D,sat}$ is the saturation coverage. (b) Fitted (solid and dashed lines) and measured (open circles) D_2 TPD spectra from a Si(011) sample with $\theta_D/\theta_{D,sat} = 1.0$. β_2 corresponds to the dideuteride phase, β_1^* to the adatom monodeuteride phase, and β_1 to the surface-atom monodeuteride phase. The linear heating rate in all experiments was $\xi = 5$ °C s^{-1}.

$\left[\begin{smallmatrix}17 & 1\\ 2 & 2\end{smallmatrix}\right]$ reconstruction and show, in addition, that the surface consists of a double-domain structure in which the two sets of domains are rotated by 73°. The two-domain nature of the ''16×2'' reconstruction is not observed in the RHEED patterns since the unit cell is nonorthogonal. Thus, only one domain is visible for a given RHEED azimuth.

Our RHEED and LEED observations show that the Si(011) surface reconstruction gradually transforms from ''16×2'' to 1×1, in agreement with previously published results,[10,11,22,23] at T_s between 700 and 725 °C. RHEED patterns obtained at temperatures within this range exhibit a continuous decrease in the intensity of the partial order reflections with increasing T_s. Figure 2 is a typical RHEED pattern obtained along the $[1\overline{1}1]$ azimuth of a 1×1 reconstructed Si(011) surface at $T_s = 750$ °C. The reflections are still sharp and distinct but there is a much higher diffuse scattering intensity due primarily to the Debye–Waller effect. The ''16×2'' to 1×1 transition was found to be reversible upon sample cooling.

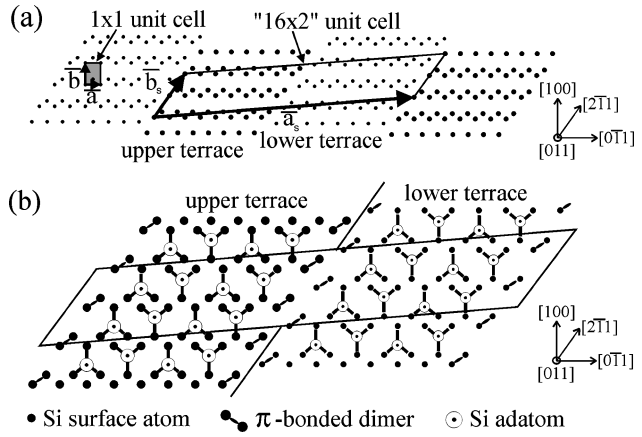

FIG. 4. (a) Bulk-terminated Si(011) with labeled 1×1 and ''16×2'' unit cells. (b) Adatom/dimer model of the Si(011)''16×2'' reconstructed surface.

TPD was used to probe atomic positions within the Si(011)''16×2'' surface unit cell.[21] Figure 3(a) is a typical set of D_2 TPD spectra from Si(011) surfaces dosed for successively longer times. The upper curve corresponds to saturation coverage $\theta_{D,sat}$. The spectra are very similar to those we obtained from Si(111)[21] and consist of a low temperature desorption peak centered at 430 °C and a high temperature feature at 550 °C. The primary difference between the Si(011) and Si(111) TPD spectra is that the high-temperature Si(011) feature contains a more obvious shoulder peak, split in this case by 30 °C and centered at 520 °C.

The Si(111)7×7 surface reconstruction has the dimer/adatom/stacking-fault structure in which Si adatoms have three backbonds to surface atoms. At low coverages on Si(111)7×7, deuterium adsorbs on the single dangling bonds of adatoms and rest atoms (first layer atoms not bonded to adatoms) giving rise to a high-temperature monodeuteride feature. Detailed analyses have shown that the two second-order Si(111)7×7 monohydride components are separated by ≃10 °C, with the higher temperature peak at 530 °C attributed to hydrogen desorption from rest atoms.[29] The Si(111) dideuteride peak at 430 °C is first observed at higher coverages as hydrogen begins to insert into adatom backbonds. Dihydride-bonded adatoms form disordered islands in which the majority species are SiH_2 with some isolated SiH_3.[30]

The position of the low-temperature peak in the Si(011) TPD spectra is almost identical to that obtained from Si(111),[21] but the splitting in the high-temperature feature is, as noted above, larger in the (011) spectra. We have fit the data using standard Polanyi–Wigner analyses.[3] Best fits were obtained using, as in the case of Si(111)7×7, one low temperature and two high temperature second-order desorption peaks while ignoring the small peak near 375 °C which we attribute to D_2 desorption from trideuteride species. An example is shown in Fig. 3(b) for a sample exposed to saturation deuterium coverage. The low temperature dideuteride peak is labeled β_2 and the two monodeuteride peaks are β_1^* and β_1. Frequency factors ν and desorption activation energies E_a are $1\times10^{15}\,s^{-1}$ and 2.22 ± 0.02 eV for β_2, $2\times10^{15}\,s^{-1}$ and 2.55 ± 0.02 eV for β_1^*, and $2\times10^{15}\,s^{-1}$ and 2.68 ± 0.02 eV for β_1.

In contrast to our Si(011) results, Si(001) TPD data is best fit using only two peaks: a low-temperature dideuteride peak centered at 405 °C and a high temperature monodeuteride peak at 515 °C.[31] While β_2 desorption from Si(001) is second order, β_1 follows first order kinetics due to π-bonding-induced pairing of dangling bonds on single dimers. However, the pairing mechanism is not expected to be important on the more open Si(011) surface. This is consistent with the observed second-order Si(011) β_1 desorption kinetics.

The bulk-terminated Si(011) surface consists of zigzag in-plane rows of atoms along $[0\bar{1}1]$ as shown in Fig. 4(a). Each surface atom has one dangling bond at an angle of 36° with respect to the surface normal. Previously suggested atomic models for the reconstructed Si(011) surface include dimers and trimers,[15] adatoms,[16,17] and adatoms plus dimers[18–20] as the building blocks. The existence of a Si(011) β_2 TPD peak at the same temperature as the β_2 peak in Si(111) spectra,[21] together with the fact that bulk-terminated (011) surface atoms have only one dangling bond, argues strongly in favor of the presence of adatoms on the reconstructed surface and against the dimer/trimer model. By analogy with the Si(111) case, we propose that Si adatom backbonds are broken to form dideuteride species during deuterium adsorption on Si(011).

After desorbing the dideuteride β_2 phase, the remaining deuterium on the Si(011) surface is present as a monodeuteride. However, the TPD spectra clearly show that the high-temperature desorption feature is composed of two peaks, β_1^* and β_1, indicating the presence of two types of monodeuterides. The Si(011) surface structure which is most consistent with our TPD results is the adatom/dimer model shown schematically in Fig. 4(b). A similar adatom/dimer foundation has been proposed for Ge(011) based upon STM observations.[32] Both the Si adatoms, giving rise to the β_1^* peak, and the surface atoms, β_1, have three backbonds and one dangling bond.

For Si(111), the difference in D_2 desorption energies from the two monohydride phases, for which the Si–H bond directions on both adatoms and rest atoms are normal to the surface, is only 0.04 eV.[29] Based upon the Si(011) surface structure model in Fig. 4(b), in which the adatom Si–H bond direction is close to normal but the surface Si–H bond is far from normal, a larger splitting in the monodeuteride desorption peaks would be expected. This is consistent with our experimental results, where the difference in Si(011) β_1^* and β_1 activation energies is 0.13 eV.

The $[\begin{smallmatrix}17 & 1\\ 2 & 2\end{smallmatrix}]$ Si(011) primitive unit cell is shown in Fig. 4. It contains 16 adatom monodeuteride species plus an additional 16 surface atom monodeuteride species generated by the D-induced breaking of the π-bonded dimers. This results in 32 dangling bonds per unit cell, compared to 64 on the unreconstructed surface. Therefore, the maximum dangling bond coverage for this surface is 0.5 ML.

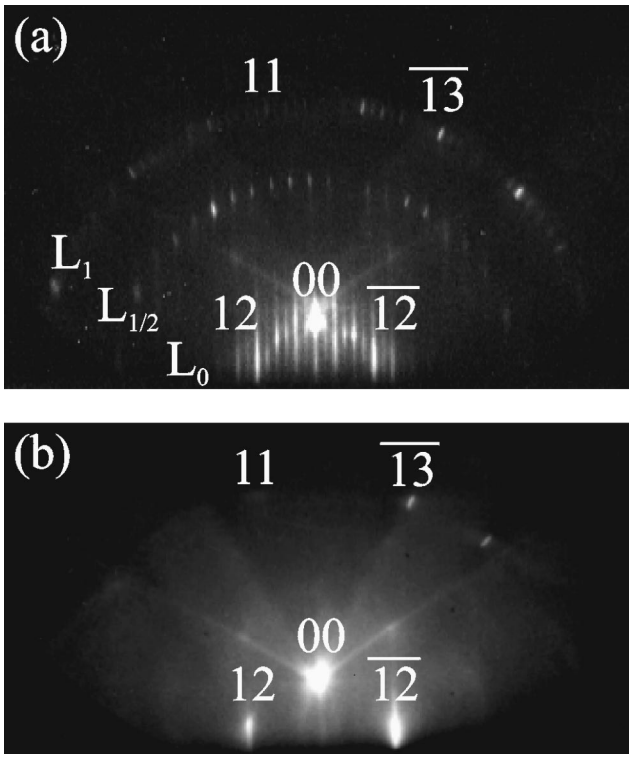

FIG. 5. RHEED patterns from a $Si_{0.78}Ge_{0.22}(011)$ layer grown at $T_s=650$ °C. The patterns were obtained along the $[1\bar{1}1]$ azimuth and are indexed as (a) ''2×8'' at 300 °C and (b) 1×1 at 800 °C.

B. $Si_{1-x}Ge_x(011)$ surface reconstructions

$Si_{1-x}Ge_x$ layers were grown on Si(011) at temperatures $T_s=400-950$ °C using a Si_2H_6 flux $J_{Si_2H_6}=2.2\times10^{16}$ $cm^{-2}s^{-1}$ and Ge_2H_6 fluxes $J_{Ge_2H_6}=0-7.8\times10^{14}$ $cm^{-2}s^{-1}$. Film thicknesses and Ge concentrations ranged from 5 to 8500 Å and 0 to 35 at %, respectively. $Si_{1-x}Ge_x(011)$ surface reconstructions were determined using *in situ* RHEED and LEED. Below a temperature-dependent critical Ge concentration x_c, the surface reconstruction of $Si_{1-x}Ge_x$ is ''16×2'', identical to that of the substrate. At Ge fractions above $x_c(T_s)$, the reconstruction transforms to ''2×8''. x_c varies from ≃0.10 at $T_s=475$ °C to 0.06 at $T_s=650$ °C and is not a function of film thickness. For $Si_{1-x}Ge_x$ films with x $>x_c$, the ''2×8'' reconstruction is obtained immediately upon initiating deposition.

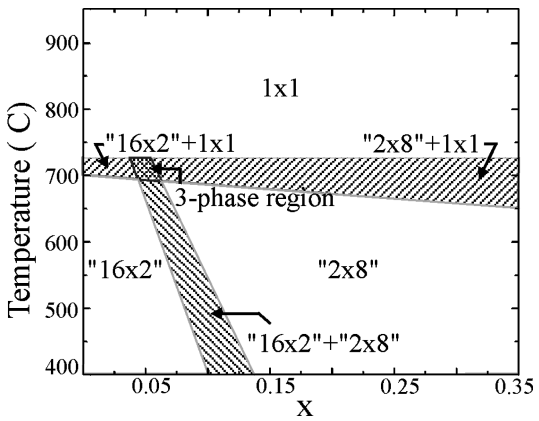

FIG. 6. A surface reconstruction phase map, plotted as a function of x and T_s, for $Si_{1-x}Ge_x(011)$ films grown on Si(011)''16×2'' at $T_s=400-950$ °C.

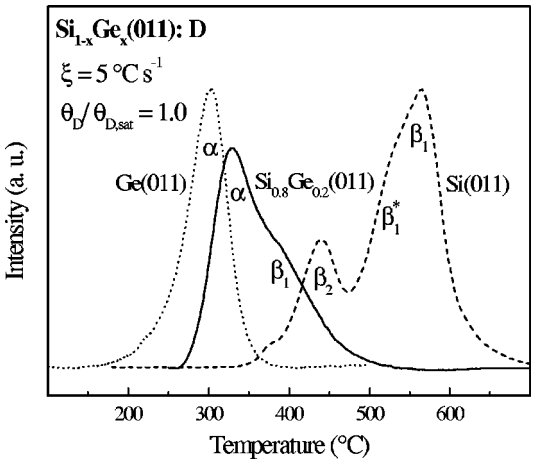

FIG. 7. A D_2 TPD spectrum from a GS-MBE $Si_{0.8}Ge_{0.2}(011)$''2×8'' layer grown at $T_s=650$ °C. Si(011)''16×2'' and Ge(011)$c8\times10$ TPD spectra are also shown for comparison. The linear heating rate in all experiments was $\xi=5$ °C s^{-1}.

Figure 5(a) is a typical ''2×8'' RHEED pattern obtained along the $[1\bar{1}1]$ azimuth, in this case from a $Si_{0.78}Ge_{0.22}$ layer grown at $T_s=650$ °C. There are seven partial-order reflections between the 00 specular reflection and the 12 and $\overline{12}$ fundamental reflections along the zero-order Laue zone L_0. The half-order reflections lie along the $L_{1/2}$ zone.

Our RHEED observations show that the $Si_{1-x}Ge_x(011)$ surface, like Si(011), transforms to a 1×1 reconstruction at temperatures between 650 and 725 °C. Figure 5(b) is a 1×1 RHEED pattern obtained at 800 °C along the $[1\bar{1}1]$ azimuth of the $Si_{0.78}Ge_{0.22}(011)$ layer corresponding to Fig. 5(a). This pattern is identical to those obtained from Si(011)1×1. The transformation between both the ''16×2'' and ''2×8'' surface reconstructions and the 1×1 is completely reversible with temperature.

Figure 6 is a surface reconstruction phase map, plotted as a function of x and T_s, for $Si_{1-x}Ge_x(011)$ films grown on Si(011) at $T_s=400-950$ °C. It shows that the composition range over which the ''16×2'' reconstruction is stable becomes increasingly narrow at higher temperatures. At $T_s=650$ °C, ''16×2'' is only obtained for samples with x between 0 and ≃0.06. Raising the temperature still further results in the gradual transition to 1×1, through a two-phase ''16×2''+1×1 region, at T_s ≃700–725 °C. The ''2×8'' to 1×1 surface phase transformation occurs over a somewhat wider temperature range extending, for example, from ≃650 to 725 °C for $Si_{0.65}Ge_{0.35}$.

While there are no published STM data on the atomic structure of the $Si_{1-x}Ge_x(011)$''2×8'' surface, insight can be gained from TPD measurements. Figure 7 is a typical D_2 TPD spectrum from a $Si_{0.8}Ge_{0.2}(011)$''2×8'' layer grown at $T_s=650$ °C. Si(011)''16×2'' and Ge(011)$c8\times10^{33}$ TPD spectra are also shown for comparison. The primary spectral feature shifts to lower temperature, from 550 °C (the β_1 monodeuteride peak) for Si(011)''16×2'' to 330 °C for $Si_{0.8}Ge_{0.2}(011)$''2×8''. In fact, the alloy TPD peak occurs quite close to the position of the α monodeuteride peak, at

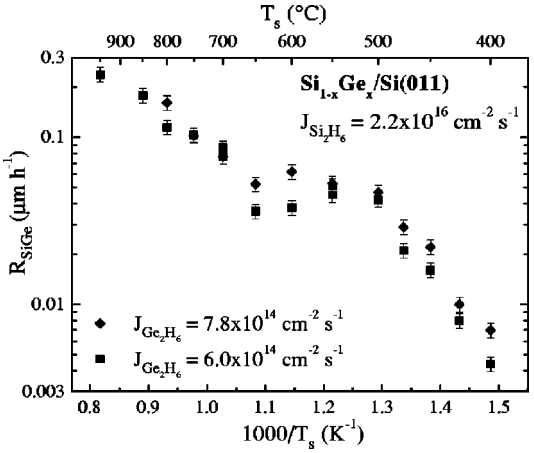

FIG. 8. GS-MBE $Si_{1-x}Ge_x(011)$ growth rates R_{SiGe} from Si_2H_6/Ge_2H_6 mixtures as a function of temperature T_s. Incident precursor fluxes were $J_{Si_2H_6}=2.2\times10^{16}$ cm^{-2} s^{-1} with $J_{Ge_2H_6}=6.0\times10^{14}$ and 7.8×10^{14} cm^{-2} s^{-1}.

300 °C, from Ge(011)$c8\times10$. This is completely analogous to TPD results from the $Si_{1-x}Ge_x/Si(001)$ system[3,4] where the very rapid decrease in the position of the monodeuteride TPD peak with increasing alloy composition is due to strong Ge surface segregation.[4] Thus, we assign the 330 °C TPD peak, labelled α, from the $Si_{0.8}Ge_{0.2}(011)$''2×8'' layer to D_2 desorption from the Ge monodeuteride phase and the high-temperature shoulder near 400 °C, labeled β_1, to D_2 desorption from the Si monodeuteride phase.

The observed decrease in Si–D surface binding energy, and the corresponding increase in the Ge–D binding energy with $Si_{1-x}Ge_x(011)$ alloy formation is, as in the case of $Si_{1-x}Ge_x(001)$,[3,4] due to long-range electronic interactions which reflect the effect of Ge (Si) alloying on the Si (Ge) band structure. Furthermore, again in analogy with GS-MBE $Si_{1-x}Ge_x(001)$,[3,4] a comparison of integrated $Si_{1-x}Ge_x(011)$ α and β_1 TPD peak intensities as a function of bulk alloy composition reveals that θ_{Ge} increases much faster than x indicating the presence of strong Ge surface segregation during $Si_{1-x}Ge_x(011)$ film growth.

C. $Si_{1-x}Ge_x(011)$ film growth kinetics

A plot of GS-MBE $Si_{1-x}Ge_x(011)$ film deposition rates R_{SiGe} as a function of $1/T_s$ is shown in Fig. 8 for films grown with a Si_2H_6 flux $J_{Si_2H_6}$ of 2.2×10^{16} cm^{-2} s^{-1} and Ge_2H_6 fluxes $J_{Ge_2H_6}$ of either 6.0×10^{14} or 7.8×10^{14} cm^{-2} s^{-1}. At $T_s\leqslant650$ °C, these fluxes correspond to film compositions within the ''2×8'' surface reconstruction regime. For deposition temperatures between $\simeq650$ and 725 °C, the surface reconstruction is two phase, ''2×8''+1×1, during growth with the 1×1 fraction increasing to 100% at $T_s\gtrsim725$ °C. Upon cooling, however, the surface reconstruction returns to pure ''2×8''. At all growth temperatures, increasing $J_{Ge_2H_6}$ from 6.0 to 7.8×10^{14} cm^{-2} s^{-1} results in an approximately proportional increase in R_{SiGe}. The Ge fraction x in alloy layers grown with $J_{Ge_2H_6}=6.0\times10^{14}$ cm^{-2} s^{-1} is 0.20 ± 0.03 while $x=0.31\pm0.02$ with $J_{Ge_2H_6}=7.8\times10^{14}$ cm^{-2} s^{-1}, independent of temperature.

Overall film growth rates R_{SiGe} in these experiments range from 0.004 μm h^{-1} at $T_s=400$ °C to 0.238 μm h^{-1} at

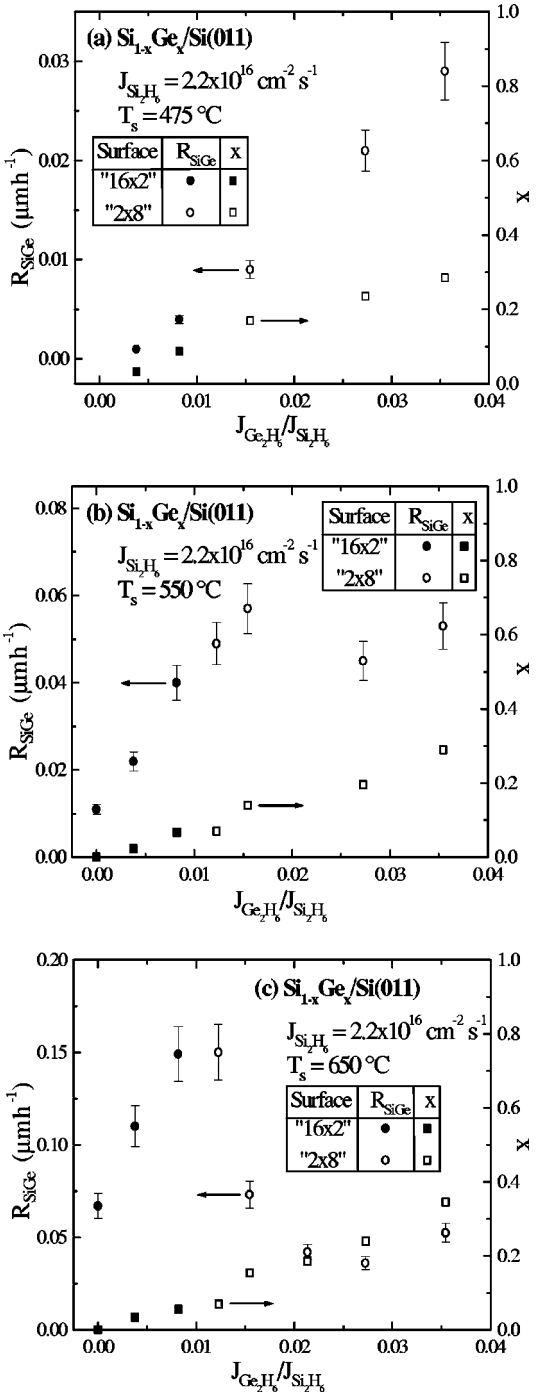

FIG. 9. GS-MBE $Si_{1-x}Ge_x(011)$ growth rate R_{SiGe} and Ge concentration x as a function of precursor flux ratio $J_{Ge_2H_6}/J_{Si_2H_6}$ at temperatures $T_s=(a)$ 475, (b) 550, and (c) 650 °C.

950 °C and are characterized by three primary temperature regimes. With $T_s\leqslant500$ °C, R_{SiGe} increases exponentially with decreasing $1/T_s$, the signature of surface-reaction-limited growth. R_{SiGe} for $Si_{1-x}Ge_x(011)$ in this mode is nearly a factor of four lower than reported $Si_{1-x}Ge_x(001)$ growth rates for layers deposited using the same precursor fluxes.[3] In the second regime, $T_s=500-650$ °C, R_{SiGe} is essentially independent of $1/T_s$, characteristic of impingement-flux-limited growth. Here, R_{SiGe} is nearly an order of magnitude lower than equivalent $Si_{1-x}Ge_x(001)$ growth rates.[3] In addition, the transition between the surface-

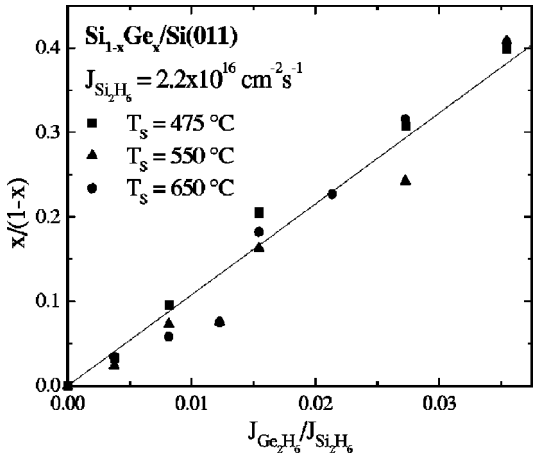

FIG. 10. The bulk composition ratio $x/(1-x)$ of GS-MBE $Si_{1-x}Ge_x(011)$ layers grown on Si(011) as a function of precursor flux ratio $J_{Ge_2H_6}/J_{Si_2H_6}$ at $T_s=475$, 550, and 650 °C.

reaction and impingement-flux-limited regimes occurs at 500 °C, compared to 600 °C for $Si_{1-x}Ge_x(001)$. Unlike the $Si_{1-x}Ge_x(001)$ case, however, R_{SiGe} for $Si_{1-x}Ge_x(011)$ increases again with a further increase in T_s. At temperatures between 650 and 725 °C, this is due to a gradual change in the surface reconstruction to 1×1, with an accompanying increase in the dangling bond density. The continued increase in R_{SiGe} at even higher growth temperatures is associated with strain-induced surface roughening as demonstrated by preliminary atomic force microscopy and XTEM investigations. We have previously reported a similar increase in the GS-MBE growth rate of Ge on Ge(001) from Ge_2H_6 due to surface roughening.[2] The enhanced deposition rate was shown to result from a combination of an increased reactive site density together with a higher digermane reactive sticking probability on the facets.

Figures 9(a)–9(c) are plots of R_{SiGe} as a function of the incident flux ratio $J_{Ge_2H_6}/J_{Si_2H_6}$ during $Si_{1-x}Ge_x(011)$ film growth at $T_s=475$, 550, and 650 °C, respectively. At $T_s=475$ °C, R_{SiGe} increases from 0.001 to 0.029 $\mu m\,h^{-1}$ as $J_{Ge_2H_6}/J_{Si_2H_6}$ is increased from 0.004 to 0.35. The ''16×2'' to ''2×8'' phase transition, which occurs over the flux ratio range $J_{Ge_2H_6}/J_{Si_2H_6}=0.008-0.012$ ($x_c=0.087-0.120$) has no apparent effect on R_{SiGe}. Since $T_s=475$ °C is well within the surface-reaction-limited regime, this indicates that the hydrogen desorption energy is less dependent on the ''16×2'' to ''2×8'' phase transition than on changes in the Ge film concentration. This can be understood from the fact that adatoms are major building blocks for both surface reconstructions.

The film growth rate increases approximately linearly with $J_{Ge_2H_6}/J_{Si_2H_6}$, at least initially, at $T_s=550$ °C in the impingement-flux-limited regime where R_{SiGe} ranges from 0.011 $\mu m\,h^{-1}$ with $J_{Ge_2H_6}/J_{Si_2H_6}=0$ to 0.057 $\mu m\,h^{-1}$ with $J_{Ge_2H_6}/J_{Si_2H_6}=0.015$. In this case, though, the surface transformation to ''2×8'' results first in a decrease in R_{SiGe} after which the growth rate remains nearly constant, with perhaps a slow increase, with increasing $J_{Ge_2H_6}/J_{Si_2H_6}$. A qualitatively similar behavior is observed at $T_s=650$ °C; R_{SiGe} increases from 0.067 $\mu m\,h^{-1}$ at $J_{Ge_2H_6}/J_{Si_2H_6}=0$ to 0.149 $\mu m\,h^{-1}$ at $J_{Ge_2H_6}/J_{Si_2H_6}=0.008$. Following the surface structural transition to ''2×8'', R_{SiGe} decreases to 0.036 $\mu m\,h^{-1}$ at $J_{Ge_2H_6}/J_{Si_2H_6}=0.027$ and increases slowly at higher flux ratios. Thus, in contrast to the surface-reaction-limited growth regime in which R_{SiGe} is not strongly dependent on the surface phase transition due in large part to the high H coverages, R_{SiGe} vs $J_{Ge_2H_6}/J_{Si_2H_6}$ exhibits an abrupt decrease at the ''16×2'' to ''2×8'' transition in the flux-limited regime. However, our TPD results indicate that there is no significant difference in the dangling bond density for the two reconstructions. Thus, the decrease in R_{SiGe} is most likely due to lower precursor reactive sticking probabilities on the ''2×8'' surface. The flux-limited film growth rate on ''2×8'' is not nearly as sensitive to increasing flux ratio as the growth rate on ''16×2''.

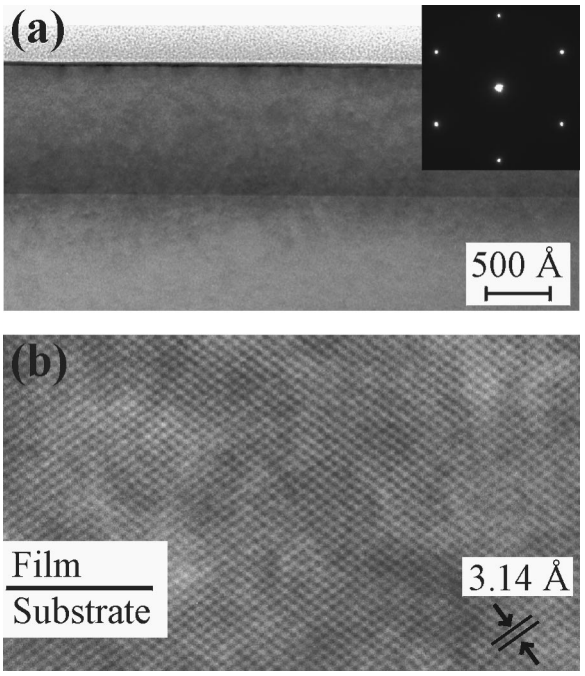

FIG. 11. (a) Bright-field XTEM micrograph obtained under two-beam diffraction conditions using a 022 diffraction vector near the $[\bar{1}11]$ zone axis of a 1010-Å-thick GS-MBE $Si_{0.93}Ge_{0.07}$ layer grown at $T_s=550$ °C. A $\bar{1}11$ selected-area diffraction pattern is shown in the inset. (b) A $\bar{1}10$ HR-XTEM image of a region near the film/substrate interface of the same sample.

The Ge concentration in as-deposited $Si_{1-x}Ge_x(011)$ alloys, also plotted in Figs. 9(a)–9(c), increases linearly with the flux ratio at all three growth temperatures. At $T_s=475$ °C, x ranges from 0.03 to 0.29 as $J_{Ge_2H_6}/J_{Si_2H_6}$ increases from 0.004 to 0.035. Nearly identical x vs $J_{Ge_2H_6}/J_{Si_2H_6}$ results were obtained at both $T_s=550$ and 650 °C in the flux-limited regime. This can be better seen in Fig. 10 in which the entire set of film composition versus flux ratio data is plotted together as $x/(1-x)$ vs $J_{Ge_2H_6}/J_{Si_2H_6}$. The slope was determined by least squares analysis to be 10.77 ± 0.35, significantly higher than the value of 7.7 obtained for $Si_{1-x}Ge_x(001)$ grown at $T_s=550$ and 800 °C.[3] This indicates that the ratio of the Ge_2H_6 to Si_2H_6 reactive sticking probabilities, while not strongly temperature dependent in either case, is higher for 011 $Si_{1-x}Ge_x$ growth.

The microstructure of fully strained $Si_{1-x}Ge_x(011)$ films was found, as judged by TEM and XTEM analyses, to be highly perfect. Typical XTEM and high-resolution XTEM (HR-XTEM) results, in this case from a 1010-Å-thick $Si_{0.93}Ge_{0.07}$ layer grown at $T_s=550\,°C$, are shown in Fig. 11. The bright-field XTEM micrograph in Fig 11(a), obtained under two-beam diffraction conditions using a 022 diffraction vector near the $[\bar{1}11]$ zone axis, is essentially featureless with the exception of the lattice-mismatch strain contrast which is clearly visible at the interface. There is no evidence of extended defects and the film surface is flat to within the resolution of the micrograph. The $\bar{1}11$ selected-area diffraction pattern shown as an insert in Fig. 11(a) consists of single-crystal reflections with uniform symmetric intensities. Figure 11(b) is a $\bar{1}10$ HR-XTEM image showing 111 lattice fringes which are continuous across the film/substrate interface.

IV. DISCUSSION

The results in Sec. III A show that the surface structure of Si(011) is complex and temperature dependent. This is of direct consequence for epitaxial $Si_{1-x}Ge_x$ growth on Si(011) since it results in the surface dangling bond density, and hence the number of available reaction sites and therefore the film deposition rate, changing dramatically with surface reconstruction. Based upon a combination of RHEED and LEED observations, we have shown that the low-temperature Si(011)''16×2'' surface reconstruction gradually and reversibly changes to 1×1 over the temperature range of 700–725 °C. From our D_2 TPD experiments combined with previous STM results,[14] the $[^{17}_{2}\,^{1}_{2}]$ surface unit cell consists of 16 adatoms and eight π-bonded dimers giving rise to 32 dangling bonds. Thus, compared to the bulk-terminated 1×1 surface, the ''16×2'' reconstruction has a maximum dangling bond coverage of 0.5 ML.

We have shown that at low Ge concentrations, the surface reconstruction of epitaxial $Si_{1-x}Ge_x(011)$ is, like that of the substrate, ''16×2''. However, for alloy films with x above a critical temperature-dependent value x_c, the reconstruction converts to ''2×8''. x_c for the ''16×2'' to ''2×8'' transition decreases continuously from $\simeq 0.10$ at $T_s=475\,°C$ to 0.06 at 650 °C. As in the case of Si(011), the surface reconstruction of $Si_{1-x}Ge_x(011)$, irrespective of whether ''16×2'' or ''2×8'' initially, gradually and reversibly transforms to 1×1 over the temperature range between $\simeq 650$ and 725 °C. A summary of observed $Si_{1-x}Ge_x(011)$ surface reconstruction as a function of alloy composition and temperature is plotted in the form of a surface structure phase map in Fig. 6.

From an analysis of our TPD results, we deduced in Sec. III B that the ''2×8'' reconstruction occurs at high Ge coverages generated by strong surface segregation during film growth. Further, the TPD results in Fig. 7 are consistent with a surface structure in which adatoms are a fundamental building block. However, a determination of local atomic positions in the surface unit cell will require additional TPD investigations combined with STM.

The experimental results in Fig. 8 show that GS-MBE $Si_{1-x}Ge_x(011)$ growth kinetics at $T_s \lesssim 650°C$ are similar to those of $Si_{1-x}Ge_x(001)$[3] in that the film deposition rate is characterized by a low-temperature surface-reaction-limited growth mode followed by a higher-temperature impingement-flux-limited regime. For the dihydride fluxes used in the present experiments, the surface reconstruction of all films in this temperature range is ''2×8''. At growth temperatures above 650 °C, additional $Si_{1-x}Ge_x(011)$ growth regimes emerge due to the gradual surface phase transition to 1×1 at $T_s=650-725\,°C$ and, at even higher temperatures, to strain-induced surface roughening. In the following discussion, we will focus primarily on the surface-reaction and flux-limited modes assuming, as in the case of $Si_{1-x}Ge_x(001)$,[3] that growth in these regimes can be described by a superposition of previously developed models for GS-MBE Si[1] and Ge[2] from Si_2H_6 and Ge_2H_6, respectively.

$R(J,T_s)$ results for Si(001)[1] and Ge(001)[2] GS-MBE are well described by a model, containing no fitting parameters, in which dissociative chemisorption of the dihydride precursor is followed by a series of fast surface decomposition reactions and H_2 desorption from the surface monohydride phase. This leads to the following growth rate equation describing both GS-MBE Si(001) and Ge(001),

$$R=\frac{2SJ\theta_{\mathrm{db}}^2}{N}, \tag{1}$$

where S is the zero-coverage reactive dihydride sticking probability, θ_{db} is the steady-state dangling bond coverage, and N is the bulk Si or Ge atom number density. Precursor reactive sticking probabilities have been measured in the flux-limited growth regime for Si_2H_6 on Si(001)[1] and for Ge_2H_6 on Ge(001).[2] The temperature dependencies of $S_{Si_2H_6}$ and $S_{Ge_2H_6}$ over the temperature range used in the film growth experiments in Refs. 1 and 2 were small and could be safely ignored. More recently, the reactive sticking probabilities of Si_2H_6 on Ge(001) and Ge_2H_6 on Si(001) have also been determined.[3]

From the above discussion, GS-MBE $Si_{1-x}Ge_x$ growth rates can be expressed as[3]

$$R_{\mathrm{SiGe}}=\frac{2\theta_{\mathrm{Si}}f_{\mathrm{db,Si}}^2}{N_{\mathrm{SiGe}}}\left(J_{Si_2H_6}S_{Si_2H_6}^{\mathrm{Si}}+J_{Ge_2H_6}S_{Ge_2H_6}^{\mathrm{Si}}\right)+\frac{2\theta_{\mathrm{Ge}}f_{\mathrm{db,Ge}}^2}{N_{\mathrm{SiGe}}}\left(J_{Si_2H_6}S_{Si_2H_6}^{\mathrm{Ge}}+J_{Ge_2H_6}S_{Ge_2H_6}^{\mathrm{Ge}}\right), \tag{2}$$

where $f_{\mathrm{db,Si}}$ and $f_{\mathrm{db,Ge}}$ are Si and Ge surface dangling bond site fractions and $S_{\mathrm{B}}^{\mathrm{A}}$ is the reactive sticking probability of the B precursor molecule on A sites. The steady-state Ge surface coverage θ_{Ge} during growth depends upon the bulk film composition together with Ge surface segregation kinetics for which the segregation enthalpy is a function of hydrogen coverage which is itself temperature-dependent.[4] We have shown by TPD that hydrogen desorption from the surface monohydride phase on $Si_{1-x}Ge_x(001)$ is second order[4] and we expect the same kinetic order for $Si_{1-x}Ge_x(011)$ where desorption from adatom sites will be limited by the rate of bimolecular recombination. Thus, the Si (Ge) dangling bond fractions f_{db} can be written as

$$f_{\mathrm{db,Si(Ge)}}=\left[1+\sqrt{\frac{2J_{\mathrm{Si_2H_6(Ge_2H_6)}}S^{\mathrm{Si(Ge)}}_{\mathrm{Si_2H_6(Ge_2H_6)}}}{N_s\nu_s\exp\left(-\frac{E_{d,\mathrm{Si(Ge)}}}{kT_s}\right)}}\right]^{-1} \quad (3)$$

in which N_s is the surface site number density [9.6×10^{14} cm^{-2} for Si(011) and 8.8×10^{14} cm^{-2} for Ge(011)], ν_s is a pre-exponential factor, and $E_{d,\mathrm{Si(Ge)}}$ is the hydrogen desorption activation energy which is a function of Ge surface coverage.[4]

Unlike the $Si_{1-x}Ge_x(001)$ system, for which detailed quantitative information is available,[1–3] little is known about individual reactive sticking probabilities and Ge surface segregation rates during GS-MBE of $Si_{1-x}Ge_x(011)$. Thus, to proceed, we make some simplifications and assumptions for the purpose of performing calculations. The $Si_{1-x}Ge_x(011)$ R_{SiGe} vs $1/T_s$ data in Fig. 8 correspond to alloy compositions $x=0.20$ for films grown with $J_{\mathrm{Ge_2H_6}}=6.0\times10^{14}$ $\mathrm{cm}^{-2}\,\mathrm{s}^{-1}$ and 0.31 with $J_{\mathrm{Ge_2H_6}}=7.8\times10^{14}$ $\mathrm{cm}^{-2}\,\mathrm{s}^{-1}$. In the analogous case of $Si_{1-x}Ge_x(001)$ growth over this composition range in the surface-reaction and flux-limited modes, θ_{Ge} varies only over a relatively narrow range. For example, θ_{Ge} ranges from 0.70 ML at $T_s=525\,^{\circ}\mathrm{C}$ to 0.82 ML at 800 °C to 0.76 ML at 950 °C with $x=0.18$.[4] This is due to competing effects. The experiments are carried out in the equilibrium segregation regime in which increasing T_s results in a decrease in θ_{Ge}. However, this is partially compensated by the fact that the hydrogen coverage also decreases with T_s thereby increasing the negative segregation enthalpy.[4]

If θ_{Ge} does not vary greatly, we can express the Si_2H_6 and Ge_2H_6 reactive sticking probabilities as average values $S^{\mathrm{SiGe}}_{\mathrm{Si_2H_6}}$ and $S^{\mathrm{SiGe}}_{\mathrm{Ge_2H_6}}$. This allows Eq. (3) to be simplified and rewritten for an average dangling bond fraction f_{db} as

$$f_{\mathrm{db}}=\left[1+\sqrt{\frac{2J_{\mathrm{Si_2H_6}}S^{\mathrm{SiGe}}_{\mathrm{Si_2H_6}}+2J_{\mathrm{Ge_2H_6}}S^{\mathrm{SiGe}}_{\mathrm{Ge_2H_6}}}{N_s\nu_s\exp\left(-\frac{E_{d(\mathrm{SiGe})}}{kT_s}\right)}}\right]^{-1}. \quad (4)$$

$E_{d(\mathrm{SiGe})}$ in Eq. (4) is the average hydrogen desorption energy. Equation (2) can now be expressed in a more usable form,

$$R_{\mathrm{SiGe}}=\frac{2f_{\mathrm{db}}^2}{N_{\mathrm{SiGe}}}\left(J_{\mathrm{Si_2H_6}}S^{\mathrm{SiGe}}_{\mathrm{Si_2H_6}}+J_{\mathrm{Ge_2H_6}}S^{\mathrm{SiGe}}_{\mathrm{Ge_2H_6}}\right). \quad (5)$$

Similarly, the steady-state composition of GS-MBE $Si_{1-x}Ge_x(011)$ can be approximated as

$$\frac{x}{1-x}=\frac{S^{\mathrm{SiGe}}_{\mathrm{Ge_2H_6}}J_{\mathrm{Ge_2H_6}}}{S^{\mathrm{SiGe}}_{\mathrm{Si_2H_6}}J_{\mathrm{Si_2H_6}}}. \quad (6)$$

Equation (6) predicts that the film composition ratio is linearly related to the flux ratio in agreement with the results in Fig. 10. From the slope of the experimental data, $S^{\mathrm{SiGe}}_{\mathrm{Ge_2H_6}}/S^{\mathrm{SiGe}}_{\mathrm{Si_2H_6}}=10.77$. R_{SiGe} has no significant growth temperature dependence over the range $T_s=475-650\,^{\circ}\mathrm{C}$. Moreover, the plot of $x/(1-x)$ vs $J_{\mathrm{Ge_2H_6}}/J_{\mathrm{Si_2H_6}}$ in Fig. 10 is continuous with little change in slope for all three growth temperatures, indicating that $S^{\mathrm{SiGe}}_{\mathrm{Ge_2H_6}}/S^{\mathrm{SiGe}}_{\mathrm{Si_2H_6}}$ remains approximately constant across the ''16×2'' to ''2×8'' phase transition.

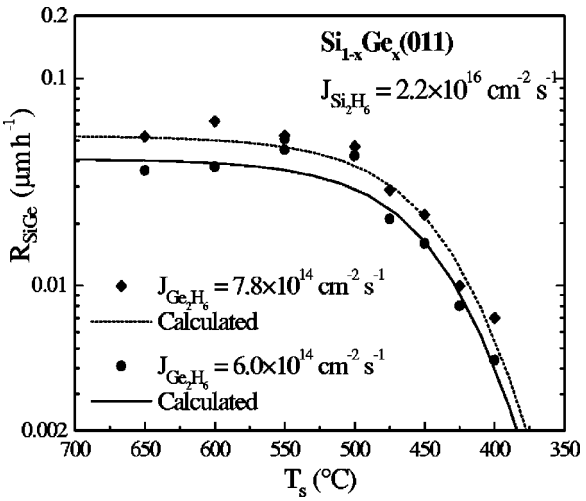

FIG. 12. Calculated (solid and dashed lines) and measured (data points) GS-MBE $Si_{1-x}Ge_x(011)$ growth rates R_{SiGe} from Si_2H_6/Ge_2H_6 mixtures as a function of temperature T_s. Incident precursor fluxes were $J_{\mathrm{Si_2H_6}}=2.2\times10^{16}$ $\mathrm{cm}^{-2}\,\mathrm{s}^{-1}$ with $J_{\mathrm{Ge_2H_6}}=6.0\times10^{14}$ and 7.8×10^{14} $\mathrm{cm}^{-2}\,\mathrm{s}^{-1}$.

At the high-temperature end of the flux-limited growth regime, f_{db} approaches unity and individual values for $S^{\mathrm{SiGe}}_{\mathrm{Si_2H_6}}$ and $S^{\mathrm{SiGe}}_{\mathrm{Ge_2H_6}}$ can be estimated by combining the result that $S^{\mathrm{SiGe}}_{\mathrm{Ge_2H_6}}/S^{\mathrm{SiGe}}_{\mathrm{Si_2H_6}}=10.77$ with Eq. (5) and the measured R_{SiGe} results in Fig. 8. This yields $S^{\mathrm{SiGe}}_{\mathrm{Si_2H_6}}=1.0\times10^{-3}$ and $S^{\mathrm{SiGe}}_{\mathrm{Ge_2H_6}}=10.8\times10^{-3}$ with $J_{\mathrm{Ge_2H_6}}=6.0\times10^{14}$ $\mathrm{cm}^{-2}\,\mathrm{s}^{-1}$. Increasing $J_{\mathrm{Ge_2H_6}}$ to 7.8×10^{14} $\mathrm{cm}^{-2}\,\mathrm{s}^{-1}$ gives $S^{\mathrm{SiGe}}_{\mathrm{Si_2H_6}}=1.2\times10^{-3}$ and $S^{\mathrm{SiGe}}_{\mathrm{Ge_2H_6}}=12.9\times10^{-3}$. Using these values for the average reactive sticking probabilities, we fit the GS-MBE R_{SiGe} vs $1/T_s$ results over the surface-reaction and flux-limited regimes. The only free parameters are ν_s and $E_{d(\mathrm{SiGe})}$. Best fits were obtained with $\nu_s=5\times10^{14}$ s^{-1} and $E_{d(\mathrm{SiGe})}=2.22$ and 2.20 eV with $J_{\mathrm{Ge_2H_6}}=6.0\times10^{14}$ and 7.8×10^{14} $\mathrm{cm}^{-2}\,\mathrm{s}^{-1}$, respectively. We used the same pre-exponential factor as reported previously for $Si_{1-x}Ge_x(001)$[3] since we showed in Sec. III A that ν_s values obtained from Si(001) and Si(011) TPD spectra were nearly identical. The fits were found to be very sensitive to the values chosen for $E_{d(\mathrm{SiGe})}$ with the goodness of fit decreasing rapidly if $E_{d(\mathrm{SiGe})}$ is changed by more than 0.01 eV. As an additional test, we used our best-fit ν_s and $E_{d(\mathrm{SiGe})}$ values to calculate peak temperatures T_p and peak shapes for the high-temperature $Si_{1-x}Ge_x(011)$ TPD features. The results were found to be in very good agreement with measured spectra. In the case of $Si_{0.8}Ge_{0.2}$ growth, for example, we calculate $T_p=404\,^{\circ}\mathrm{C}$ while in Fig. 7, T_p is $\simeq400\,^{\circ}\mathrm{C}$. The agreement provides additional confidence in the validity of the growth model.

The calculated and experimental curves in Fig. 12 exhibit quite good agreement. The results show that $E_{d(\mathrm{SiGe})}$ decreases with increasing $J_{\mathrm{Ge_2H_6}}$ and, hence, increasing Ge concentration in the alloy layer. This is consistent with our previous $Si_{1-x}Ge_x(001)$ results showing that the hydrogen

desorption energy decreases with increasing θ_{Ge} due primarily to a weakening of Si–H bonds through long-range electronic interactions.[4]

Unlike the $Si_{1-x}Ge_x(001)$ case, however, Fig. 8 shows that $Si_{1-x}Ge_x(011)$ growth rates increase again at higher deposition temperatures in the flux-limited regime. This is due to an increase in the surface dangling bond density as the surface structure gradually changes from a ''2×8'' reconstruction to bulk-terminated 1×1 over the temperature range between ≃650 and 725 °C. Indeed, the results show that R_{SiGe} increases sharply over this growth temperature range. As T_s is increased still further, R_{SiGe} continues to increase. This, we propose, is associated with surface roughening. Initial atomic force microscopy investigations show that strong strain-induced roughening, already detectable as increased diffuse scattering in RHEED patterns from $Si_{1-x}Ge_x(011)$, becomes significant at $T_s \gtrsim 725$ °C.

V. CONCLUSIONS

TPD was used to show that the Si(011)''16×2'' reconstructed unit cell is composed of 16 adatoms and eight π-bonded dimers, resulting in a maximum dangling bond coverage of 0.5 ML. The surface reconstruction of $Si_{1-x}Ge_x(011)$ overlayers grown on Si(011) remains ''16×2'' at low Ge concentrations but transforms to ''2×8'' at a critical x value which decreases from ≃0.10 at $T_s = 475$ °C to 0.06 at $T_s = 650$ °C. At even higher temperatures, both Si(011) and $Si_{1-x}Ge_x(011)$ surfaces gradually and reversibly transform to 1×1. The transformation is complete at ≃725 °C. We showed, based upon analyses of TPD results, that the ''2×8'' surface occurs at high Ge coverages generated by strong surface segregation during film growth. Further, the TPD results are consistent with a surface structure in which Si and Ge adatoms are fundamental components in the ''2×8'' reconstruction.

GS-MBE $Si_{1-x}Ge_x(011)$ growth kinetics in the surface-reaction and flux-limited regimes are well described by a model in which dissociative chemisorption of the dihydride precursors is followed by a series of surface decomposition reactions and second-order H_2 desorption. In the surface-reaction-limited regime ($T_s \leqslant 500$ °C), R_{SiGe} decreases exponentially with $1/T_s$ and is rate-limited by H_2 desorption from the adatom and surface atom monohydride phases but is not affected by the ''16×2'' to ''2×8'' surface transformation. At $T_s = 500$–650 °C, in the impingement-flux-limited regime, R_{SiGe} is limited by precursor reactive sticking probabilities which are essentially independent of T_s. In this growth mode, R_{SiGe} increases linearly with $J_{Ge_2H_6}/J_{Si_2H_6}$ but at a higher rate for growth on the ''16×2'' than the ''2×8'' surface reconstruction. The ratio of the Ge_2H_6 to Si_2H_6 reactive sticking probabilities was found to be constant, 10.77, at $T_s = 475$–650 °C. Thus, $x/(1-x)$ increases linearly with increasing $J_{Ge_2H_6}/J_{Si_2H_6}$ in both the surface-reaction-limited and impingement-flux-limited regimes. At higher growth temperatures, R_{SiGe} once again increases with increasing T_s. Initially, at $T_s = 650$–725 °C, this is due to a gradual change in the surface reconstruction to 1×1 with a corresponding increase in the maximum dangling bond density from 0.5 to 1.0 ML. The continued increase in R_{SiGe} at even higher T_s is associated with strain-induced surface roughening.

ACKNOWLEDGMENTS

The authors gratefully acknowledge the support of the Office of Naval Research under a contract administered by Dr. Larry Cooper, the U.S. Department of Energy Division of Materials Sciences under Award DEFG02-ER9645439, and the Semiconductor Research Corporation. P. Desjardins is partially supported by the Natural Sciences and Engineering Research Council of Canada (NSERC). We also appreciate the use of the Center for Microanalysis of Materials at the University of Illinois, which is partially supported by the U.S. Department of Energy.

[1] T. R. Bramblett, Q. Lu, T. Karasawa, M.-A. Hasan, S. K. Jo, and J. E. Greene, J. Appl. Phys. **76**, 1884 (1994).
[2] T. R. Bramblett, Q. Lu, N.-E. Lee, N. Taylor, M.-A. Hasan, and J. E. Greene, J. Appl. Phys. **77**, 1504 (1995).
[3] H. Kim, N. Taylor, T. R. Bramblett, and J. E. Greene, J. Appl. Phys. (in press).
[4] H. Kim, N. Taylor, J. R. Abelson, and J. E. Greene, J. Appl. Phys. **82**, 6062 (1997); H. Kim, P. Desjardins, J. R. Abelson, and J. E. Greene, Phys. Rev. B **58**, 4803 (1998).
[5] C. W. Liu, J. C. Sturm, Y. R. J. Lacroix, M. L. W. Thewalt, and D. D. Perovic, Appl. Phys. Lett. **65**, 76 (1994).
[6] T. L. Kreifels, R. L. Hengehold, Y. K. Yeo, P. E. Thomson, and D. S. Simons, J. Vac. Sci. Technol. A **13**, 636 (1995).
[7] R. Hull, J. C. Bean, L. Peticolas, and D. Bahnck, Appl. Phys. Lett. **59**, 964 (1991).
[8] F. Jona, IBM J. Res. Dev. **9**, 375 (1965).
[9] B. Z. Olshanetsky and A. A. Shklyaev, Surf. Sci. **67**, 581 (1977).
[10] T. Ichinokawa, H. Ampo, S. Miura, and A. Tamura, Phys. Rev. B **31**, 5183 (1985).
[11] Y. Yamamoto, S. Ino, and T. Ichikawa, Jpn. J. Appl. Phys., Part 2 **25**, L331 (1986).
[12] H. Ampo, S. Miura, K. Kato, Y. Ohkawa, and A. Tamura, Phys. Rev. B **34**, 2329 (1986).
[13] S. Miura, K. Kato, T. Ide, and T. Ichinokawa, Surf. Sci. **191**, 259 (1987).
[14] E. J. van Loenen, D. Dijkkamp, and A. J. Hoeven, J. Microsc. **152**, 487 (1988).
[15] Y. Yamamoto, Phys. Rev. B **50**, 8534 (1994).
[16] R. S. Becker, B. S. Swartzentruber, and J. S. Vickers, J. Vac. Sci. Technol. A **6**, 472 (1988).
[17] E. G. Klein, H. Wormeester, and A. van Silfhout, J. Vac. Sci. Technol. A **8**, 2747 (1990).
[18] A. I. Shkrebtii, C. M. Bertoni, R. Del Sole, and B. A. Nesterenko, Surf. Sci. **239**, 227 (1990).
[19] B. A. Nesterenko and A. I. Shkrebtii, Surf. Sci. **213**, 309 (1989).
[20] B. A. Nesterenko, Appl. Surf. Sci. **33/34**, 21 (1988).
[21] H. Kim, N. Taylor, T. Spila, G. Glass, S. Y. Park, J. E. Greene, and J. R. Belson, Surf. Sci. **380**, L496 (1997).
[22] G. Shimaoka, Appl. Surf. Sci. **65/66**, 569 (1993).
[23] Y. Yamamoto, T. Sueyoshi, T. Sato, and M. Iwatsuki, Jpn. J. Appl. Phys., Part 2 **32**, L532 (1993).
[24] R. Butz and H. Lüth, Surf. Sci. **365**, 807 (1996).
[25] T. R. Bramblett, Ph.D. thesis, University of Illinois, 1994.
[26] X.-J. Zhang, G. Xue, A. Agarwal, R. Tsu, M.-A. Hasan, J. E. Greene, and A. Rockett, J. Vac. Sci. Technol. A **11**, 2553 (1993).
[27] L. R. Doolittle, Nucl. Instrum. Methods Phys. Res. B **9**, 344 (1985).
[28] E. A. Wood, J. Appl. Phys. **35**, 1306 (1964).
[29] M. C. Flowers, N. B. H. Jonathan, Y. Liu, and A. Morris, J. Chem. Phys. **102**, 1034 (1995).
[30] J. J. Boland, Surf. Sci. **244**, 1 (1991).
[31] H. Kim, G. Glass, S. Y. Park, T. Spila, N. Taylor, J. R. Abelson, and J. E. Greene, Appl. Phys. Lett. **69**, 3869 (1996).
[32] T. Ichikawa, T. Sueyosi, Y. Sato, M. Iwatsuki, F. Udagawa, and I. Sumita, Solid State Commun. **93**, 541 (1995).
[33] H. Kim and J. E. Greene (unpublished).